ANALYSIS OF CROSS FRACTURE SEEPAGE CHARACTERISTICS UNDER DIFFERENT ANGLE CONDITIONS

by

Zun-Dong YANG [a,b], ***Jing XIE*** [c*], ***and Hu-Chao DENG*** [d]

[a] Sichuan University – The Hong Kong Polytechnic University Institute for Disaster Management and Reconstruction, Sichuan University, Chengdu, China
[b] State Key Laboratory of Intelligent Construction and Healthy Operation and Maintenance of Deep Underground Engineering, Sichuan University, Chengdu, China
[c] College of Water Resource and Hydropower, Sichuan University, Chengdu, Sichuan, China
[d] Yalong River Hydropower Development Co., Ltd., Chengdu, China

Original scientific paper
https://doi.org/10.2298/TSCI2502237Y

Based on the Weierstrass-Mandelbrot fractal function, multiple X-shaped fracture models with different intersection angles were established to investigate the fracture seepage characteristics under both equal and unequal inlet pressure conditions. The results showed that the intersection angle of the fractures influenced the flow contribution of each inlet branch to the rough and smooth outlet fractures, as well as the degree of convergence at the intersection.

Key words: *X-shaped fractures, fracture seepage, convergence, fractal dimension, intersection angle*

Introduction

As resource extraction gradually moved to deeper levels, the study of fracture seepage patterns in media such as rocks and coal seams became increasingly important [1-4]. However, the deep environment and stress conditions are highly complex, with factors such as temperature, pressure, and fluid media creating a variety of intricate scenarios [5-8]. The development of fractures is controlled by multiple factors and exhibits strong randomness, making the fluid-flow and particle transport between fractures even more complicated [9-12].

Extensive research has explored fracture seepage in rock media, particularly how inlet pressure, intersection angle, and roughness affect fluid-flow at fracture intersections [13, 14]. Xie *et al.* [15] used 3-D printing to create intersecting fractures with different fractal dimensions, quantifying pressure drop losses and competitive flow splitting. Tang *et al.* [16] studied *Y*-shaped fractures through numerical simulations, analyzing competitive flow splitting via fluid streamlines. Yang *et al.* [17] applied the Weierstrass-Mandelbrot function model *X*-shaped fractures, examining seepage characteristics under different flow modes, fractal dimensions, and inlet pressures. However, the variable intersection angles in underground rock masses require further investigation.

This study used the Weierstrass-Mandelbrot function model *X*-shaped fractures and analyzed their seepage characteristics under varying intersection angles and inlet pressures. Numerical simulations were conducted for three fracture scenarios under both equal and unequal

* Corresponding author, e-mail: xiejing200655@163.com

inlet pressures, focusing on flow contributions from the inlets to outlets with different fractal dimensions.

Model building

This study took the commonly encountered *X*-shaped fractures in the field of geology as the starting point, fig. 1, and established three different scenarios, with the intersection angles of the fractures set at 30°, 60°, and 90°. For each scenario, 13 different inlet pressure conditions were applied, while the outlet pressure was set to 0. The flow mode was set to convection, the average aperture was set to 0.5 mm, the straight length was set to 100 mm. Specific parameters are provided in tab. 1.

Table 1. Parameters of intersecting fractures

Parameters	Water pressure of Inlet 1 [Pa]	Water pressure of Inlet 2 [Pa]	Water pressure ratio (Inlet 1/Inlet 2)
Experimental conditions	50	50	1
	100	100	1
	150	150	1
	200	200	1
	250	250	1
	50	100	1/2
	100	150	2/3
	150	200	3/4
	200	250	4/5
	250	200	5/4
	200	150	4/3
	150	100	3/2
	100	50	2/1

In this study, the Weierstrass-Mandelbrot function is used to model the *X*-shaped fracture, and the function is expressed:

$$W(t) = \sum_{n=-\infty}^{\infty} (1 - \mathrm{e}^{ib^n t})\mathrm{e}^{i\varphi_n} / b^{(2-D)n} \tag{1}$$

where b is the real number greater than 1, reflecting the degree of deviation of the curve from a straight line, φ_n – the arbitrary phase angle, and $D \in (1, 2)$ – the fractal dimension. By selecting the real part (cosine function) of the function $W(t)$ as the fractal function, the expression is obtained:

$$C(t) = \mathrm{Re}\,W(t) = \sum_{n=-\infty}^{\infty} (1 - \cos b^n t) / b^{(2-D)n} \tag{2}$$

This function represents a fractal curve that is continuous everywhere, and non-differentiable, and has a fractal dimension D. The fractal dimension D satisfies the relation:

$$D_{\mathrm{HB}} - \frac{B}{b} \le D \le D_{\mathrm{HB}} \tag{3}$$

where B is the constant and D_{HB} – the Hausdorff-Besicovitch dimension. The fractal function $C(t)$ uses the parameter $b = 1.4$. A fractal curve is generated using MATLAB, and the smooth

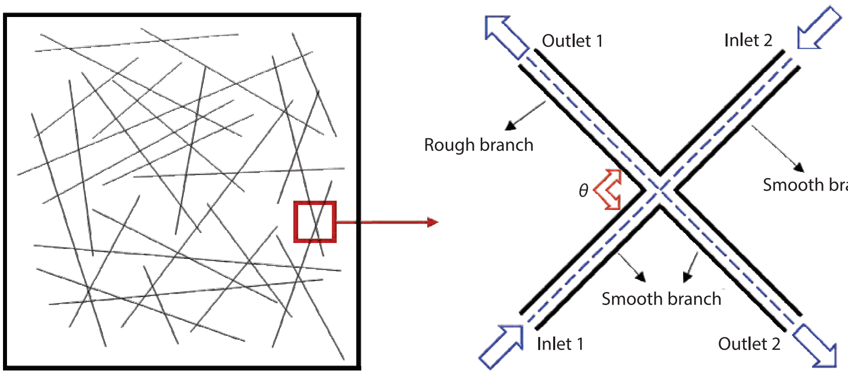

Figure 1. Schematic diagram of intersecting fractures

and rough fractures within the intersecting fracture model are constructed. The fractal dimension of the smooth fracture is set to 1.0, while the fractal dimension of the rough fracture is set to 1.2. The specific model is presented on fig. 2.

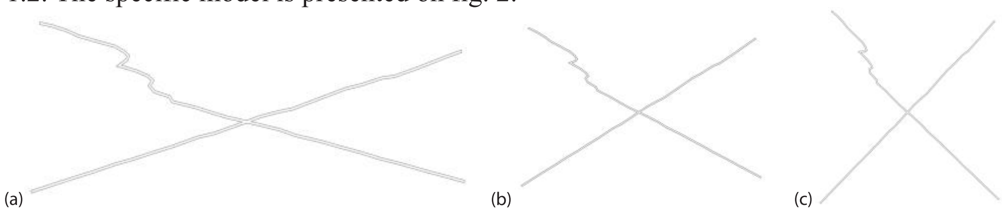

Figure 2. Fracture models at different angles; (a) 30°, (b) 60°, and (c) 90°

Numerical simulations of all the scenarios involved previously were carried out using COMSOL Multiphysics 6.0. The fluid density and dynamic viscosity were set $1 \cdot 10^3$ kg/m^3, $1.01 \cdot 10^{-3}$ Pa·s.

Result and discussion

Seepage characteristics analysis under the same pressure conditions

With equal inlet pressures, the relationship between fracture flow and inlet pressure at different angles showed an approximately linear growth trend, fig. 3. The rough (R-outlet, fractal dimension 1.2) had lower flow than the smooth (S-outlet, fractal dimension 1.0), with a distribution of 47.3% and 52.7%, respectively. While the intersection angle did not affect overall flow distribution, it influenced each inlet branch's contribution the outlets and the degree of convergence at the intersection.

The contribution of Inlet 1 and Inlet 2 to the two outlets is discussed below. In COMSOL, the size-controlled streamline method was used, with denser streamlines representing higher velocities and sparser streamlines indicating lower velocities. This method was employed to distribute flow between the inlets. For example, at 250-250 Pa, velocity contour and streamline plots were generated. As shown in figs. 4 and 5, when inlet pressures were the same, an increase in the fracture intersection angle led to greater convergence in the intersection region. At a 30° intersection angle, flow from both inlets favored the outlet with a smaller intersection angle, resulting in a shorter flow path. However, at a 90° intersection angle, the flow distribution between the two outlets became balanced, with equal flow from both inlets. At this point, only the fractal dimension of the outlet fracture branches influenced the flow distribution.

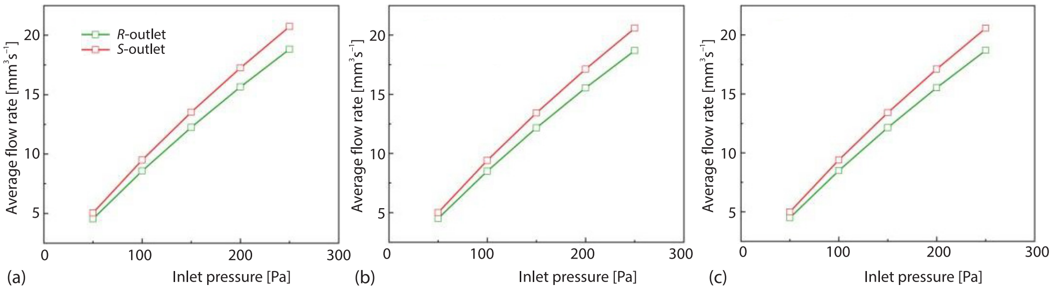

Figure 3. The average flow rate with inlet pressure under the same pressure conditions; (a) 30°, (b) 60°, and (c) 90°

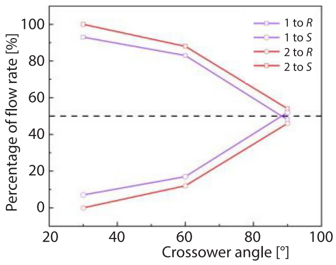

Figure 4. The contribution of each inlet flow to the flow at each outlet under the same pressure conditions

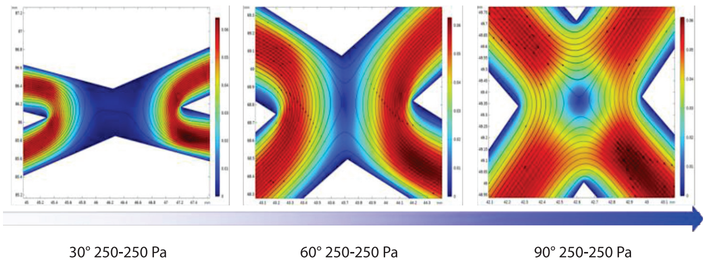

Figure 5. Velocity and streamline plots of intersecting fractures at different angles under the same pressure conditions

Characteristics analysis under different pressure conditions

When the inlet pressures differed, the pressure ratio influenced the flow distribution between the two inlet and two outlet flows. As shown in fig. 6, for intersection angles of 30° or 60°, if the flow from Inlet 1 was smaller than from Inlet 2, the entire flow from Inlet 1 was directed to the rough fracture branch (with the smaller intersection angle), resulting in a shorter flow path. The flow from Inlet 2 predominantly entered the smooth fracture branch. As the pressure ratio increased, more flow from Inlet 2 was directed to the smooth fracture branch, while less flow entered the rough fracture branch. This suggested that as the fluid velocity increased, the smooth fracture's competitive flow splitting capacity strengthened. When the pressure ratio became large enough, the entire flow from Inlet 2 went to the smooth fracture, while the majority of the flow from Inlet 1 entered the rough fracture branch, with only a small portion flowing into the smooth fracture. As the pressure ratio continued to increase, the flow into the smooth fracture branch increased, while the flow into the rough fracture branch decreased, indicating that the smooth fracture increasingly competed for flow from Inlet 1.

When the intersection angle was 90°, it could be seen that the flow from the branch with the lower inlet pressure was evenly distributed between the rough fracture branch and the smooth fracture branch. The flow from the branch with the higher inlet pressure was more likely to enter the smooth fracture branch than the rough fracture branch. This indicated that, for fractures with a 90° intersection angle, the flow at the rough and smooth fracture branch outlets primarily depended on the flow distribution from the branch with the higher inlet pressure. The smooth fracture branch, compared to the rough fracture branch, competed for and received more flow.

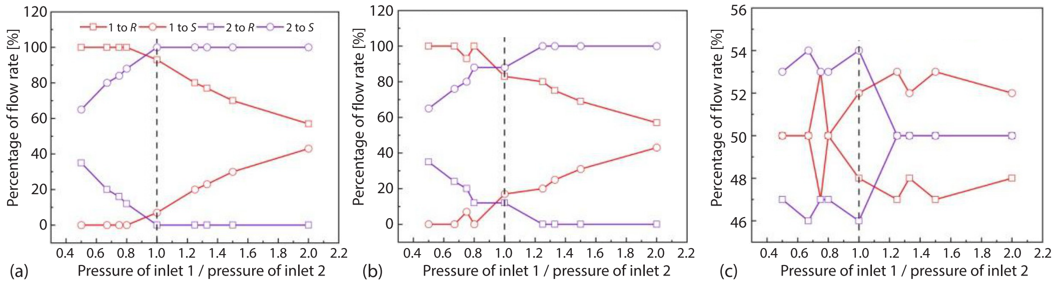

Figure 6. The contribution of each inlet flow to the flow at each outlet under different pressure conditions; (a) 30°, (b) 60°, and (c) 90°

Conclusion

The intersection angle of the fractures did not affect the overall competitive flow splitting ability between rough and smooth fractures but influenced the flow contribution from each inlet branch and the degree of convergence at the intersection. With equal inlet pressures, a larger intersection angle enhanced convergence and increased the flow distribution ratio to both outlets. When inlet pressures differed, flow from the lower-pressure branch was entirely directed to the outlet with a smaller intersection angle. As the pressure ratio increased, more flow from the higher-pressure branch was directed to the smooth outlet.

Acknowledgment

This work was financially supported by the National Key Research and Development Program of China (2023YFF0615401) and National Natural Science Foundation of China (52225403; 42377143; U2013603).

Nomenclature

φ_n – any phase angle, [°]

D – fractal dimension, [–]

References

[1] Gao, M., *et al.*, Mechanical Behaviors of Segments in Small Curvature Radius Intervals of Shield Tunnels: From Field Monitoring to Laboratory Testing, *Rock Mechanics and Rock Engineering*, *56* (2023), 11, pp. 8115-8134

[2] Gao, M., *et al.*, Mechanical Behavior of Coal under Different Mining Rates: A Case Study from Laboratory Experiments to Field Testing, *International Journal of Mining Science and Technology*, *31* (2021), 5, pp. 825-841

[3] Gao, M., *et al.*, Fractal Evolution And Connectivity Characteristics of Mining-Induced Crack Networks in Coal Masses at Different Depths, *Geomechanics and Geophysics for Geo-Energy and Geo-Resources*, *7* (2021), 9

[4] Gao, M.-Z., *et al.*, The Mechanism of Microwave Rock Breaking and Its Potential Application Rock-Breaking Technology In Drilling, *Petroleum Science*, *19* (2022), 3, pp. 1110-1124

[5] Gao, Y., *et al.*, The Novel Strength Criterion and the Associated Constitutive Model Based on the Finite Deformation Behavior for the Rock under the Disturbance Stress Paths, *Geomechanics for Energy and the Environment*, *34* (2023), ID100456

[6] Gao, Y., *et al.*, The Acoustic Emission Behavior and Its Fractal Characteristics of the Sandstone under the Disturbance Stress Paths, *Rock Mechanics and Rock Engineering*, *56* (2023), 8, pp. 5487-5511

[7] Gao, Y., *et al.*, The Strata Movement and Ground Pressure under Disturbances from Extra Thick Coal Seam Mining: A Case Study of a Coal Mine in China, *Geomechanics and Geophysics for Geo-Energy and Geo-Resources*, *8* (2022), 6, ID199

[8] Gao, Y., *et al*., Does Double Pre-Notches Have a Greater Impact Than Single Pre-Notch on the Mechanical and Fracture Behavior of Rock, Insights from Three-Point Bending Tests Using the Numerical Approach of Grain-Based Model, *Theoretical and Applied Fracture Mechanics*, *133* (2024), ID104624
[9] Mingzhong, G., *et al*., Discing Behavior and Mechanism of Cores Extracted from Songke-2 Well at Depths Below 4500 m, *International Journal of Rock Mechanics and Mining Sciences*, *149* (2022), ID104976
[10] Wang, Y., *et al.*, Microwave Assistance Effect for Rock Breaking of TBM Disc Cutter Using the Coupled Method of Continuum and Grain-Based Model, *Engineering Analysis with Boundary Elements*, *159* (2024), Feb., pp. 466-484
[11] Yang, B.-G., *et al*., Exploration of Weakening Mechanism of Uniaxial Compressive Strength of Deep Sandstone under Microwave Irradiation, *Journal of Central South University*, *29* (2022), 2, pp. 611-623
[12] Zhang, Y., *et al*., Multi-Stage Evolution of Pore Structure of Microwave-Treated Sandstone: Insights From Nuclear Magnetic Resonance, *International Journal of Rock Mechanics and Mining Sciences*, *183* (2024), ID105952
[13] Zhang, S., *et al*., Quantitative Evaluation of the Onset and Evolution for the Non-Darcy Behavior of the Partially Filled Rough Fracture, *Water Resources Research*, *60* (2024), 3, IDe2023WR036494
[14] Zhang, S., Liu, X. J. W.R. R., A Semi-Analytical Solution for the Equivalent Permeability Coefficient of the Multilayered Porous Medium with Continuous Fracture, *Water Resources Research*, *60* (2024), 2, IDe2023WR036203
[15] Xie, J., *et al*., Fluid-flow Characteristics of Cross-Fractures with Two Branch Fractures of Different Roughness Controlled by Fractal Dimension: An Experimental Study, *Journal of Petroleum Science and Engineering*, *196* (2021), ID107996
[16] Tang, R., *et al*., Research on Seepage Characteristics of Y-Shaped Fractures under Different Fracture Roughness, *Geofluids*, *2022* (2022), 1, ID7521955
[17] Yang, Z.-D., *et al*., Study On Seepage Characteristics of Cross Fractures in Adjacent and Convective Flow Modes, *Thermal Science*, *27* (2023), 1B, pp. 527-535

Paper submitted: September 1, 2024
Paper revised: November 10, 2024
Paper accepted: November 22, 2024